





Generation of 56.5 W femtosecond laser radiation by the combination of an Nd-doped picosecond amplifier and multi-pass-cell device

JIAJUN SONG,^{1,2} LIYA SHEN,^{2,3} JIANYU SUN,^{2,4}
ZHAOHUA WANG,¹  ZHIYI WEI,¹  YUJIE PENG,^{2,*} 
AND YUXIN LENG^{2,5}

¹Beijing National Laboratory for Condensed Matter Physics, Institute of Physics, Chinese Academy of Sciences, Beijing 100190, China

²State Key Laboratory of High Field Laser Physics and CAS Center for Excellence in Ultra-intense Laser Science, Shanghai Institute of Optics and Fine Mechanics, Chinese Academy of Sciences, Shanghai 201800, China

³School of Physical Science and Technology, ShanghaiTech University, Shanghai 201210, China

⁴Center of Materials Science and Optoelectronics Engineering, University of Chinese Academy of Sciences, Beijing 100049, China

⁵lengyuxin@mail.siom.ac.cn

*yjpeng@siom.ac.cn

Abstract: We demonstrate the generation of high average power femtosecond laser radiation by combination of an Nd-doped picosecond amplifier and a multi-pass cell device. With this efficient and robust scheme, the pulse duration of a picosecond amplifier is compressed from 9.13 ps to 477 fs, corresponding to a compression factor of 19.1. The average power before and after pulse compression is 77 W and 56.5 W respectively, so the overall transmission reaches 73.4%. The presented scheme offers a viable route toward low-cost and simple configuration high power femtosecond lasers driven by Nd-doped picosecond amplifiers.

© 2022 Optica Publishing Group under the terms of the [Optica Open Access Publishing Agreement](#)

1. Introduction

High repetition rate and high average power femtosecond lasers are powerful tools for researching material processing [1–3]. The Ti: Sapphire crystal has been an excellent gain medium for the generation of femtosecond laser pulse for many years due to its good optical and mechanical properties, such as wide emission spectral bandwidth (~500 nm) and high thermal conductivity. However, the Ti: Sapphire femtosecond amplifiers typically employed frequency doubled Q-switched nanosecond lasers as the pump source, which increases the cost and footprint of these laser systems. Besides, the available pump power and large quantum defect of the Ti: Sapphire crystal strongly limits the repetition rate to several kilohertz and average power to 20 W level of the Ti: Sapphire amplifiers [4,5].

Compared with the Ti: Sapphire crystal, ytterbium (Yb)-doped gain mediums offer the advantages of low quantum defect and can be directly pumped with the high-power laser diode (LD). Therefore, high power femtosecond lasers, whose generation is based on the Yb-doped gain mediums in architectures of bulk [6], fiber [7,8], thin disk [9,10], Innoslab [11] and single crystal fiber [12,13], have developed rapidly in the last few years. In particular, Yb: fiber femtosecond amplifier based on coherent combination technology can deliver 10.4 kW average power [8]. Nevertheless, the Yb-doped gain mediums like thin disk, Innoslab, photonic crystal fiber and rod fiber are almost monopolized by a few companies and research institutes. They are technically complex and expensive. Moreover, high-power femtosecond lasers with hundreds of microjoules or millijoules pulse energy are beneficial to certain material processing applications. To get it,

the chirped pulse amplification (CPA) technology could be applied, which further increases the cost, footprint and technical complexity of the high power Yb-doped laser systems.

It is the same with Yb-doped gain mediums that neodymium (Nd)-doped gain mediums like Nd: YVO₄ or Nd: YAG also feature the low quantum defect and direct LD pumped configuration. Limited by emission spectral bandwidth, the mode locked Nd: YVO₄ or Nd: YAG lasers typically deliver ~10 ps pulses directly. Therefore, the pulse energy of the picosecond laser could be amplified to hundreds of microjoules or millijoules with a CPA free architecture [14–16]. Compared with the Yb-doped femtosecond amplifiers with the similar pulse energy, the stretcher and compressor containing expensive dispersive elements like gratings or chirped fiber Bragg gratings can be omitted. Consequently, the Nd-doped picosecond amplifiers give the advantages of simple configuration, low cost, and small footprint. Although their power scalability is not as good as that of Yb: fiber, Yb: Innoslab and Yb: thin disk lasers, many companies still can offer compact and reliable picosecond amplifiers with several hundred watts output. Thus, combining high average power Nd-doped picosecond lasers with high efficiency nonlinear pulse compression technologies, it is more feasible to obtain high-power femtosecond lasers with the same merit of the Nd-doped picosecond amplifiers.

Noble gas-filled hollow-core fiber [17–19], solid thin plates [20–22], photonic crystal fiber [23,24], Kagome photonic crystal fiber [25–27] and multi-pass cell (MPC) [28–38] are well-known spectral broadening schemes. Among them, the MPC, first demonstrated by Jan Schulte *et al.* in 2016 [28] stands out with high efficiency and simple configuration. It only comprises two concave mirrors with the same radius of curvature R and the nonlinear elements placed between them. And they are cheaper and easier to get. The distance L between two mirrors is satisfying $0 < L < 2R$ to form a resonator. Therefore, A shorter R typically means a smaller MPC size. Further, the MPC could be folded by additional plane mirrors to make it more compact [39].

For a Gaussian-shaped pulse, the spectral broadening factor F is given by [40]:

$$F = \frac{\Delta\omega_{out}}{\Delta\omega_{in}} = \sqrt{1 + \frac{4}{3\sqrt{3}}B^2} = \sqrt{1 + (0.88B)^2}$$

where $\Delta\omega_{in}$ and $\Delta\omega_{out}$ denote the rms spectral bandwidths of the laser pulse before and after spectral broadening, and B means the total nonlinear phase shift in the nonlinear interaction process [41]. For a large nonlinear phase shift, the F is approximately proportional to B : $F \approx 0.88B$ [41]. The nonlinear phase shift per pass inside the MPC is small so that the self-focusing or spatio-spectral couplings is avoidable and the spatial profile mostly remains Gaussian [30,42]. After several round trips, the nonlinearity can be largely accumulated and dramatic spectral broadening can be realized.

The MPC also features great power and energy handling capabilities. In 2020, Christian Grebing *et al.* compressed the pulse duration of a kilowatt coherently combined Yb: fiber amplifier from 200 fs to 31 fs by MPC scheme [36], making the MPC become the first nonlinear pulse compression method at kilowatt average power level. Scaling the input pulse energy of the MPC to 10 millijoules level reported in 2018, Martin Kaumanns *et al.* compressed the pulse duration of an 18 mJ thin-disk amplifier from 1.3 ps to 41 fs with an efficiency of 95.7% [31]. Three years later, they improved the input pulse energy to a record 112 mJ by transforming the input laser beam from Gaussian mode to the first order helical Laguerre–Gaussian mode [43].

By nonlinear pulse compression of the Nd-doped picosecond laser based on the MPC devices J. Song *et al.* have been performed the generation of 172 fs pulses by cascading two stage MPCs in 2021 [44]. Nevertheless, the efficiency of that system was just 51%, which results in an output power of only 117 mW [44]. And multi-stage MPCs also suffers other complications, such as intricate configuration and large footprint. In the same year, we performed the generation of 601 fs pulse by combination of a Nd: YVO₄ regenerative amplifier and single stage MPC device, but the generated femtosecond laser was just 1.23 W [45].

In this work, we focus on scaling the power of femtosecond lasers generated from Nd-doped picosecond amplifiers and pulse shorting capability of single stage MPC devices. The generation of femtosecond laser radiation with 56.5 W average power and 477 fs pulse duration by post compression of an Nd-doped picosecond amplifier in a single-stage solid state MPC is proposed and performed. And the resulting femtosecond laser features excellent beam spatial profile and power stability. Presented laser source has great potential to be applied in the micromachining.

2. Experimental setup

The schematic of the experimental setup is depicted in Fig. 1. A fiber solid-state hybrid picosecond amplifier is employed as the driving laser, which mainly consists of a mode-locked fiber picosecond oscillator, an acoustic optical modulator for pulse picker, multi-stage fiber pre-amplifiers and multi-stage Nd: YVO₄ main amplifiers. The driving laser delivers 77 W average power at 700 kHz repetition rate. And the size of the driving laser is 900 mm(length)×420 mm(width)×212 mm(height). The central wavelength and spectral full width at half maximum (FWHM) of the driving laser is 1064.5 nm and 0.215 nm, respectively, as shown in Fig. 2(a). Assuming a Gaussian-shaped pulse, the pulse duration of the picosecond laser is 9.13 ps (FWHM), as shown in Fig. 2(b). A half-wave plate (HWP) and a thin-film polarizer (TFP) form an adjustable attenuator to control the power into the MPC. The q-parameter of the picosecond laser is mode-matched to the eigenmode of the MPC by three lenses (L1-L3). The MPC is composed of two concave mirrors (CM1-CM2) with 76.2 mm diameter and 300 mm radius of curvature. The MPC mirrors are high reflection coated at the central wavelength of 1064 nm with a reflectivity near 99.95%. And they are not dispersive mirrors. Two mirrors are separated by 535 mm, which generates the eigenmode diameter distribution of 1.08 mm on the MPC mirrors and 0.355 mm in the middle of the MPC. One piece of anti-reflection (AR) coated fused silica plate (transmittance of AR coating is around 99.95%) with a thickness of 25 mm and diameter of 2 inches is specifically selected as the nonlinear element to mitigate the residual reflection losses. The plate is positioned about 7 cm away from the focus to avoid optical damage. The beam from the picosecond laser is coupled in and out of the MPC by two rectangular mirrors, the size of 3 mm×10 mm. By fine-tuning the cavity length, the number of passes through the plate can be reached to 111. The corresponding optical length is estimated to be 2.775 m in the fused silica plate and 56.6 m in air. The circle's radius of reflections on the MPC mirrors is about 28 mm. The laser beam from the MPC is collimated with a lens L4. The chirp removal is

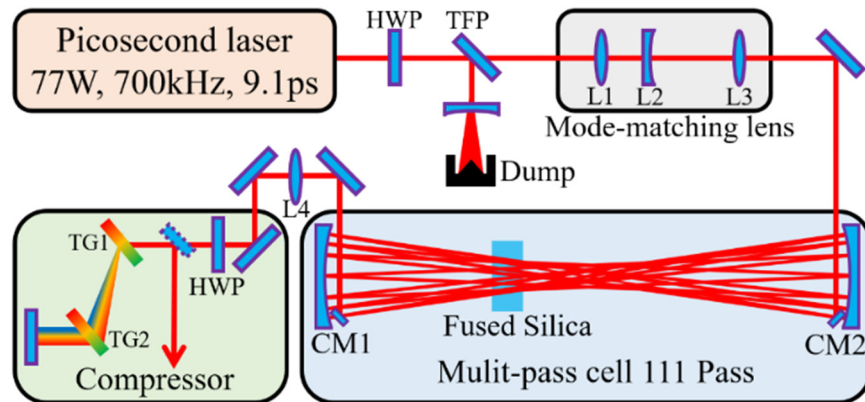


Fig. 1. Experimental setup realizing nonlinear pulse compression for high average power picosecond laser. HWP, half-wave plate; TFP, thin-film polarizer; L1-L4, lenses; CM1-CM2, concave mirrors; TG1-TG2, transmission gratings.

subsequently implemented by a pair of transmission gratings (TG1-TG2) with 1200 line/mm groove (1692-28 × 23-6.35-H, Gitterwerk). A HWP is inserted before the grating pair compressor to rotate the polarization of the picosecond laser for optimizing the diffraction efficiency.

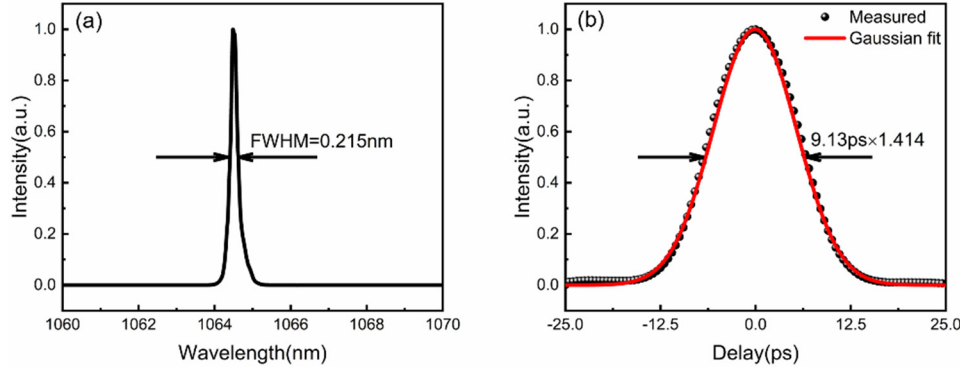


Fig. 2. Characterization of the picosecond laser pulses. (a) Spectrum. (b) Measured intensity autocorrelation trace (black dot) and Gaussian fit (red curve).

3. Experimental results

The maximum output power of the MPC is 64.5 W at an incident power of 77 W, corresponding to a transmission efficiency of 83.8%. It is dominated by linear losses including 110 reflections on the MPC mirrors and 111 passes through the fused silica plate. This part losses can be estimated to be $1 - 0.9995^{332} = 15.3\%$. Other optical components can also cause small losses such as the residual reflectivity of the mode matching lenses. And input/output rectangular mirrors may clip the laser beam slightly [30]. The dispersion length L_d of the fused silica is calculated to be 1.82 km for the input pulse, which is much longer than the propagation length (2.775 m) mentioned above. Therefore, the pulse duration of the picosecond laser is barely broadened by the material dispersion and pulse propagating through the MPC can be treated as dispersion free. But the single-pass nonlinear phase shift still decreases gradually owing to the losses from each pass. The average peak power of the picosecond laser is about 11 MW. Taking into account of the energy losses and the beam quality (M^2) of the picosecond laser, the average focal length of the Kerr-lens generated by the nonlinear element is estimated to be 1.5 m, which changes the eigenmode diameter from 0.447 mm to 0.44 mm at the position of the nonlinear element. The single pass and total beam averaged nonlinear phase shift is estimated to be 0.086π and 9.55π , respectively. After nonlinear interaction, the spectral bandwidth is broadened to 6.1 nm at the intensity of half the outer spectral maxima (AQ6374, YOKOGAWA), as shown in Fig. 3(a), which yields a broadening factor of 28.4. The broadened spectrum with an intensity modulation is the result of self-phase modulation. And the intensity of the newly generated sidelobe is lower than the initial central part, which is similar with the results of the Ref. [34]. We attribute this phenomenon to the poor temporal contrast of the input picosecond pulse. The amplified spontaneous emission, pre-pulses and post-pulses of the input laser are not spectrally shifted due to their low peak power [31]. The Fourier transform limit (FTL) pulse duration (FWHM) of the broadened spectrum is 466 fs, as depicted in the inset of Fig. 3(a), which leads to an attainable compression factor of 19.6. It is close to the theoretical compression factor given by $\tau_{in}^{FWHM} / \tau_{out}^{FWHM} = \varphi_{total}^{nl} / \sqrt{e} = 18.2$ under the assumption of Gaussian-shaped pulse [36], where τ_{in}^{FWHM} denotes the input pulse duration, τ_{out}^{FWHM} means the FTL of the broadened spectrum and φ_{total}^{nl} is the total nonlinear phase shift in the MPC. Due to the intensity modulation of the

broadened spectrum, the calculated FTL pulse appears some side pulses around the main pulse. By integration, we estimate that 81.6% energy is concentrated in the main pulse.

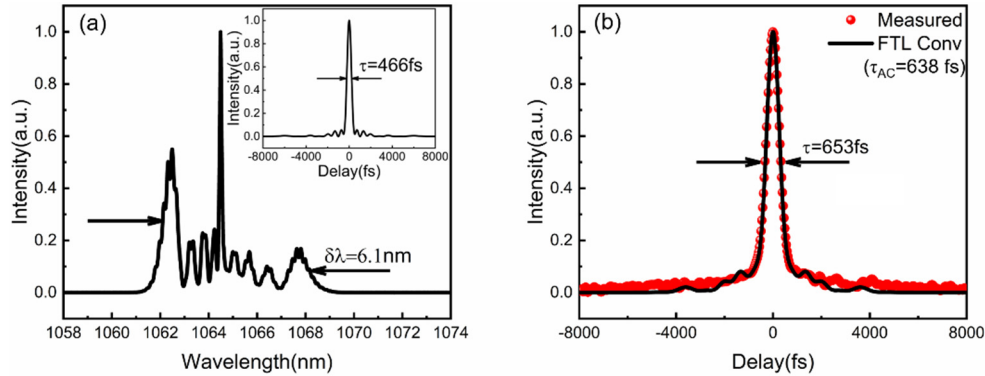


Fig. 3. Characterization of the laser pulses after pulse compression. (a) Broadened spectrum. Inset, calculated FTL pulse duration. (b) Measured intensity autocorrelation trace after the grating pair compressor (red dot) and the convolution of the FTL pulse (black curve).

The pulses from the MPC are incident on the gratings at a Littrow angle of 39.7° to maximize diffraction efficiency. The remaining power after the grating pair compressor is 56.5 W, corresponding to an efficiency of 87.6%. As a result, the overall transmission of the system is 73.4%, obviously lower than the ones of the other single stage MPC device ($\sim 90\%$). Two reasons contribute to this result. Firstly, there are more round trips in our MPC. Secondly, the efficiency of the grating pair compressor is lower than the chirped mirrors employed in previous articles. However, it is reasonable to remove the chirp by grating pair because the required group delay dispersion in our experiment is at the magnitude of 10^6 fs^2 , and the chirped mirrors are difficult to meet this function. The shortest autocorrelation trace (FWHM) of 653 fs is measured via a commercial intensity autocorrelator (PulseCheck-50, A. P. E. GmbH), as shown in Fig. 3(b) (red dot). And the calculated autocorrelation trace of the FTL pulse (FWHM) is 638 fs, also shown in Fig. 3(b) (black curve), producing a deconvolution factor of 0.73. Assuming that the deconvolution factor of the compressed pulse is same as the FTL [29], a compressed pulse duration (FWHM) of 477 fs is inferred, corresponding to a pulse compression factor of 19.1. From the pedestal area of the autocorrelation trace, we estimate that 65% pulse energy is in the main pulse [34,36]. Therefore, the peak power after nonlinear pulse compression reaches to 110 MW. The compressed pulse duration is slightly longer than that of the FTL, which may be attributed to the high order dispersion generated by the grating pair compressor and the fiber pre-amplifier of the picosecond laser.

The M^2 values before and after the MPC is 1.49×1.53 and 1.62×1.56 (BSQ-SP300, Ophir Spiricon), as shown in Fig. 4. The near field and far field beam profiles after MPC are presented in the inset of Fig. 4(b). The beam quality after MPC is almost preserved but slightly degraded. This may be attributed to two reasons. Firstly, the aberration of the Kerr lenses in the 25 mm thick fused silica plate affects the beam quality [28]. Secondly, the imperfections of the mirror shape would also deteriorate the beam quality owing to the picosecond laser 110 reflections on the MPC mirrors [31].

Figure. 5 presents the long-term power stability at the output of the MPC, which is stable with a root-mean-square (RMS) 0.62% over 1 hour.

Without any housing to isolate the MPC device nor any actuators to actively stabilize the beam pointing, the beam pointing stability over 1 hour is characterized by a beam analyzer (WinCamD-LCM, DataRay). The data acquisition rate is 1 Hz and the results are shown in

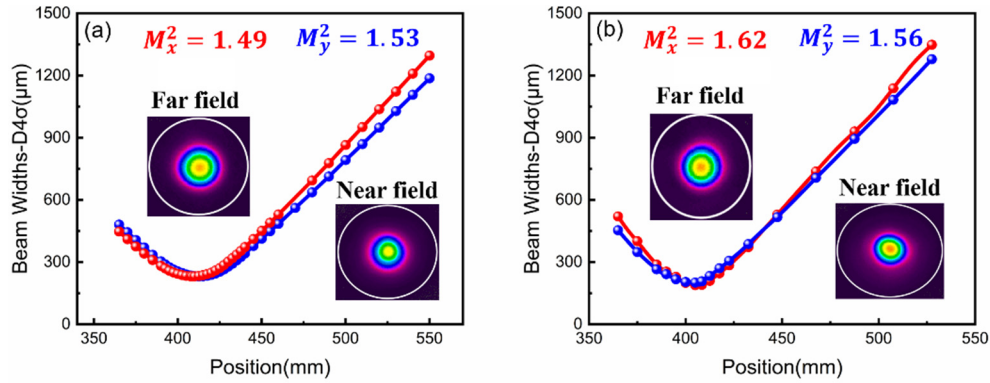


Fig. 4. Beam quality of the picosecond laser. (a) The M^2 before the MPC. Inset, Beam profile at near-field and far-field. (b) The M^2 after the MPC. Inset, Beam profile at near-field and far-field.

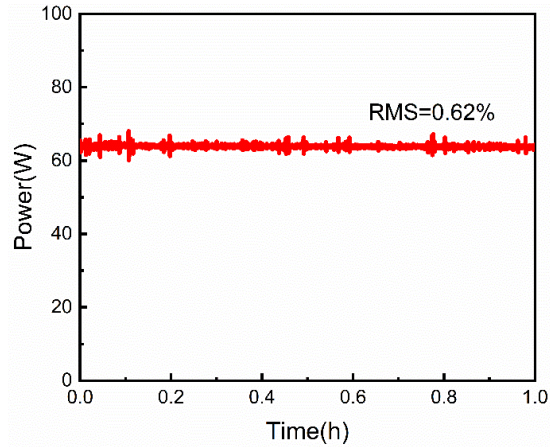


Fig. 5. The power stability at the output of the MPC.

Fig. 6(a). And the beam angular deviation distribution is presented in Fig. 6(b). The RMS beam pointing stability is $12.2 \mu\text{rad}$ in the horizontal and $11 \mu\text{rad}$ in the vertical direction. It can be seen that the beam pointing stability is good enough after MPC device. At the same time, the beam position stability is also characterized, the results shown in Fig. 6(c). And the beam position deviation distribution is presented in Fig. 6(d). The RMS of the beam position deviation is $121 \mu\text{m}$ in the horizontal and $118 \mu\text{m}$ in the vertical direction. Therefore, for a $3.6 \text{ mm} \times 3.7 \text{ mm}$ beam size at $1/e^2$ intensity, the RMS stability of the beam position is 3.36% in the horizontal and 3.19% in the vertical direction. The beam position fluctuation after the MPC device is a little dramatic, which attribute to the long optical path of the MPC, air agitation, vibration of the optical platform and heat deposition in the MPC mirrors. In the future, the actuators would be employed into the system to stabilize the beam pointing and position [30].

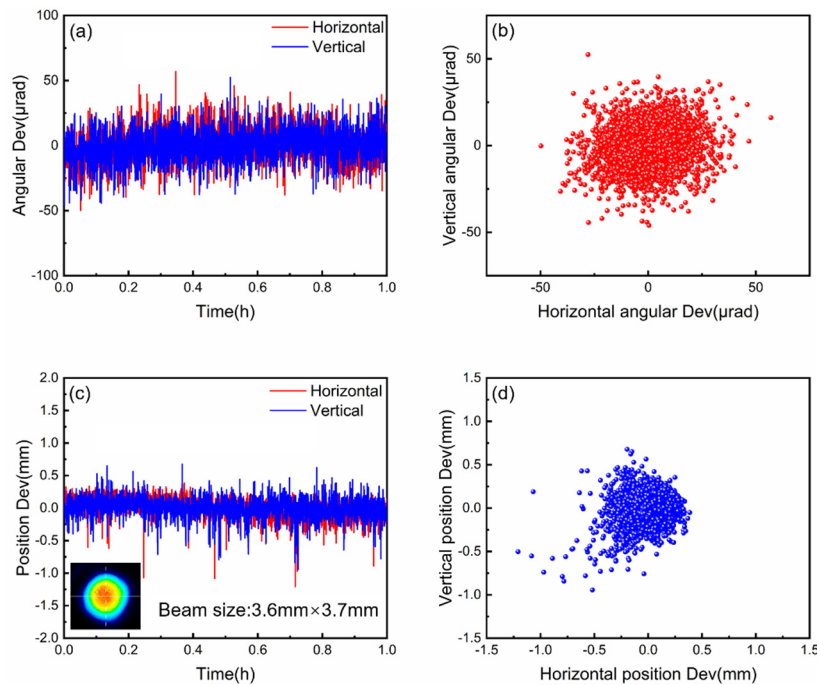


Fig. 6. The beam pointing and position stability at the output of the MPC. (a) The beam angular deviation fluctuation in horizontal (red curve) and vertical (blue curve) directions within one hour. (b) Collected beam angular deviation distribution. (c) The beam position deviation fluctuation in horizontal (red curve) and vertical (blue curve) directions within one hour. Inset, beam profile at the output of the MPC. (d) Collected beam position deviation distribution.

4. Summary

In summary, the generation of high-power femtosecond laser with low cost and simple configuration is implemented by combination of a 77 W picosecond amplifier and high efficiency all-bulk MPC device. A femtosecond laser with an average power of 56.5 W, pulse duration of 477 fs, beam quality of 1.62×1.56 , and stable power of 0.62% RMS is produced. The total efficiency of the system is 73.4%. Presented scheme has great potential to attain higher power femtosecond laser sources driven by Nd-doped picosecond amplifiers.

Funding. National Key Research and Development Program of China (2017YFE0123700); National Natural Science Foundation of China (61925507); Shanghai Rising-Star Program (21QA1410200); National Natural Science Foundation of China (62075227); Youth Innovation Promotion Association of the Chinese Academy of Sciences (2020248).

Disclosures. The authors declare no conflicts of interest.

Data availability. Data underlying the results presented in this paper are not publicly available at this time but may be obtained from the authors upon reasonable request.

References

1. S. S. Liang, H. Q. Ye, and F. S. Yuan, "Changes in Crystal Phase, Morphology, and Flexural Strength of As-Sintered Translucent Monolithic Zirconia Ceramic Modified by Femtosecond Laser," *Appl. Sci.-Basel* **11**, 1 (2021).
2. L. Shah, M. E. Fermann, J. W. Dawson, and C. P. J. Barty, "Micromachining with a 50 W, 50 μ J, sub-picosecond fiber laser system," *Opt. Express* **14**(25), 12546–12551 (2006).
3. M. Kahmann, R. Gebbs, R. Fleischhaker, I. Zawischa, J. Kleinbauer, S. Russ, L. Bauer, U. Keller, B. Faisst, A. Budnicki, and D. Sutter, "Non-infrared femtosecond lasers: Status and prospects," in *Conference on Frontiers in Ultrafast Optics - Biomedical, Scientific, and Industrial Applications XVI*, Proceedings of SPIE 2016),

4. V. Bagnoud and F. Salin, "Amplifying laser pulses to the terawatt level at a 1-kilohertz repetition rate," *Appl. Phys. B* **70**(S1), S165–S170 (2000).
5. B. Langdon, J. Garlick, X. Ren, D. J. Wilson, A. M. Summers, S. Zigo, M. F. Kling, S. Lei, C. G. Elles, E. Wells, E. D. Poliakov, K. D. Carnes, V. Kumarappan, I. Ben-Itzhak, and C. A. Trallero-Herrero, "Carrier-envelope-phase stabilized terawatt class laser at 1 kHz with a wavelength tunable option," *Opt. Express* **23**(4), 4563–4572 (2015).
6. U. Demirbas, H. Cankaya, Y. Hua, J. Thesinga, M. Pergament, and F. X. Kartner, "20-mJ, sub-ps pulses at up to 70 W average power from a cryogenic Yb:YLF regenerative amplifier," *Opt. Express* **28**(2), 2466–2479 (2020).
7. M. Muller, A. Klenke, A. Steinkopff, H. Stark, A. Tunnermann, and J. Limpert, "3.5 kW coherently combined ultrafast fiber laser," *Opt. Lett.* **43**(24), 6037–6040 (2018).
8. M. Muller, C. Aleshire, A. Klenke, E. Haddad, F. Legare, A. Tunnermann, and J. Limpert, "10.4 kW coherently combined ultrafast fiber laser," *Opt. Lett.* **45**(11), 3083–3086 (2020).
9. C. Herkommer, P. Krotz, R. Jung, S. Klingebiel, C. Wandt, R. Bessing, P. Walch, T. Produit, K. Michel, D. Bauer, R. Kienberger, and T. Metzger, "Ultrafast thin-disk multipass amplifier with 720 mJ operating at kilohertz repetition rate for applications in atmospheric research," *Opt. Express* **28**(20), 30164–30173 (2020).
10. F. Saltarelli, I. J. Graumann, L. Lang, D. Bauer, C. R. Phillips, and U. Keller, "Power scaling of ultrafast oscillators: 350-W average-power sub-picosecond thin-disk laser," *Opt. Express* **27**(22), 31465–31474 (2019).
11. P. Russbueldt, T. Mans, J. Weitenberg, H. D. Hoffmann, and R. Poprawe, "Compact diode-pumped 1.1 kW Yb:YAG Innoslab femtosecond amplifier," *Opt. Lett.* **35**(24), 4169–4171 (2010).
12. V. Markovic, A. Rohrbacher, P. Hofmann, W. Pallmann, S. Pierrot, and B. Resan, "160 W 800 fs Yb:YAG single crystal fiber amplifier without CPA," *Opt. Express* **23**(20), 25883–25888 (2015).
13. F. Beirou, M. Eckerle, T. Graf, and M. A. Ahmed, "Amplification of radially polarized ultra-short pulsed radiation to average output powers exceeding 250 W in a compact single-stage Yb:YAG single-crystal fiber amplifier," *Appl. Phys. B* **126**(9), 148 (2020).
14. Y. Chen, K. Liu, J. Yang, F. Yang, H. W. Gao, N. Zong, L. Yuan, Y. Y. Lin, Z. Liu, Q. J. Peng, Y. Bo, D. F. Cui, and Z. Y. Xu, "8.2mJ, 324MW, 5kHz picosecond MOPA system based on Nd: YAG slab amplifiers," *J. Opt.* **18**, 6 (2016).
15. Z. L. Zhang, Q. Liu, P. Yan, P. Xia, and M. L. Gong, "Laser diode end-pumped Nd:YVO₄ regenerative amplifier for picosecond pulses," *Chin. Phys. B* **22**, 5 (2013).
16. Z. G. Peng, M. Chen, C. Yang, L. Chang, and G. Li, "A cavity-dumped and regenerative amplifier system for generating high-energy, high-repetition-rate picosecond pulses," *Jpn. J. Appl. Phys.* **54**(2), 028001 (2015).
17. B. H. Chen, M. Kretschmar, D. Ehberger, A. Blumenstein, P. Simon, P. Baum, and T. Nagy, "Compression of picosecond pulses from a thin-disk laser to 30fs at 4W average power," *Opt. Express* **26**(4), 3861–3869 (2018).
18. S. Bohman, A. Suda, T. Kanai, S. Yamaguchi, and K. Midorikawa, "Generation of 5.0 fs, 5.0 mJ pulses at 1 kHz using hollow-fiber pulse compression," *Opt. Lett.* **35**(11), 1887–1889 (2010).
19. C. F. Dutin, A. Dubrouil, S. Petit, E. Mevel, E. Constant, and D. Descamps, "Post-compression of high-energy femtosecond pulses using gas ionization," *Opt. Lett.* **35**(2), 253–255 (2010).
20. C. H. Lu, Y. J. Tsou, H. Y. Chen, B. H. Chen, Y. C. Cheng, S. D. Yang, M. C. Chen, C. C. Hsu, and A. H. Kung, "Generation of intense supercontinuum in condensed media," *Optica* **1**(6), 400–406 (2014).
21. P. He, Y. Y. Liu, K. Zhao, H. Teng, X. K. He, P. Huang, H. D. Huang, S. Y. Zhong, Y. J. Jiang, S. B. Fang, X. Hou, and Z. Y. Wei, "High-efficiency supercontinuum generation in solid thin plates at 0.1 TW level," *Opt. Lett.* **42**(3), 474–477 (2017).
22. M. Seo, K. Tsendsuren, S. Mitra, M. Kling, and D. Kim, "High-contrast, intense single-cycle pulses from an all thin-solid-plate setup," *Opt. Lett.* **45**(2), 367–370 (2020).
23. W. Liu, C. Li, Z. G. Zhang, F. X. Kartner, and G. Q. Chang, "Self-phase modulation enabled, wavelength-tunable ultrafast fiber laser sources: an energy scalable approach," *Opt. Express* **24**(14), 15328–15340 (2016).
24. W. Liu, S. H. Chia, H. Y. Chung, R. Greinert, F. X. Kartner, and G. Q. Chang, "Energetic ultrafast fiber laser sources tunable in 1030–1215 nm for deep tissue multi-photon microscopy," *Opt. Express* **25**(6), 6822–6831 (2017).
25. F. Emaury, C. J. Saraceno, B. Debord, D. Ghosh, A. Diebold, F. Gerome, T. Sudmeyer, F. Benabid, and U. Keller, "Efficient spectral broadening in the 100-W average power regime using gas-filled kagome HC-PCF and pulse compression," *Opt. Lett.* **39**(24), 6843–6846 (2014).
26. F. Guichard, A. Giree, Y. Zaouter, M. Hanna, G. Machinet, B. Debord, F. Gerome, P. Dupriez, F. Druon, C. Honninger, E. Mottay, F. Benabid, and P. Georges, "Nonlinear compression of high energy fiber amplifier pulses in air-filled hypocycloid-core Kagome fiber," *Opt. Express* **23**(6), 7416–7423 (2015).
27. B. Debord, M. Alharbi, L. Vincetti, A. Husakou, C. Fourcade-Dutin, C. Hoenninger, E. Mottay, F. Gerome, and F. Benabid, "Multi-meter fiber-delivery and pulse self-compression of milli-Joule femtosecond laser and fiber-aided laser-micromachining," *Opt. Express* **22**(9), 10735–10746 (2014).
28. J. Schulte, T. Sartorius, J. Weitenberg, A. Vernaleken, and P. Russbueldt, "Nonlinear pulse compression in a multi-pass cell," *Opt. Lett.* **41**(19), 4511–4514 (2016).
29. J. Weitenberg, T. Saule, J. Schulte, and P. Russbueldt, "Nonlinear Pulse Compression to Sub-40 fs at 4.5 mJ Pulse Energy by Multi-Pass-Cell Spectral Broadening," *IEEE J. Quantum Electron.* **53**(6), 1–4 (2017).
30. J. Weitenberg, A. Vernaleken, J. Schulte, A. Ozawa, T. Sartorius, V. Pervak, H. D. Hoffmann, T. Udem, P. Russbueldt, and T. W. Hansch, "Multi-pass-cell-based nonlinear pulse compression to 115 fs at 7.5 μ J pulse energy and 300 W average power," *Opt. Express* **25**(17), 20502–20510 (2017).

31. M. Kaumanns, V. Pervak, D. Kormin, V. Leshchenko, A. Kessel, M. Ueffing, Y. Chen, and T. Nubbemeyer, "Multipass spectral broadening of 18 mJ pulses compressible from 1.3 ps to 41 fs," *Opt. Lett.* **43**(23), 5877–5880 (2018).
32. K. Fritsch, M. Poetzlberger, V. Pervak, J. Brons, and O. Pronin, "All-solid-state multipass spectral broadening to sub-20 fs," *Opt. Lett.* **43**(19), 4643–4646 (2018).
33. L. Lavenu, M. Natile, F. Guichard, Y. Zaouter, X. Delen, M. Hanna, E. Mottay, and P. Georges, "Nonlinear pulse compression based on a gas-filled multipass cell," *Opt. Lett.* **43**(10), 2252–2255 (2018).
34. P. Russbueltd, J. Weitenberg, J. Schulte, R. Meyer, C. Meinhardt, H. D. Hoffmann, and R. Poprawe, "Scalable 30 fs laser source with 530 W average power," *Opt. Lett.* **44**(21), 5222–5225 (2019).
35. P. Balla, A. Bin Wahid, I. Sytceovich, C. Guo, A. L. Viotti, L. Silletti, A. Cartella, S. Alisauskas, H. Tavakol, U. Grosse-Wortmann, A. Schonberg, M. Seidel, A. Trabattoni, B. Manschwetus, T. Lang, F. Calegari, A. Couairon, A. L'Huillier, C. L. Arnold, I. Hartl, and C. M. Heyl, "Postcompression of picosecond pulses into the few-cycle regime," *Opt. Lett.* **45**(9), 2572–2575 (2020).
36. C. Grebing, M. Muller, J. Buldt, H. Stark, and J. Limpert, "Kilowatt-average-power compression of millijoule pulses in a gas-filled multi-pass cell," *Opt. Lett.* **45**(22), 6250–6253 (2020).
37. E. Vicentini, Y. C. Wang, D. Gatti, A. Gambetta, P. Laporta, G. Galzerano, K. Curtis, K. McEwan, C. R. Howle, and N. Coluccelli, "Nonlinear pulse compression to 22 fs at 15.6 μ J by an all-solid-state multipass approach," *Opt. Express* **28**(4), 4541–4549 (2020).
38. S. Gröbmeyer, K. Fritsch, B. Schneider, M. Poetzlberger, V. Pervak, J. Brons, and O. Pronin, "Self-compression at 1 μ m wavelength in all-bulk multi-pass geometry," *Appl. Phys. B* **126**(10), 159 (2020).
39. H. PeterRussbueltd, Johannes Weitenberg, Aachen, Andreas Vernaleken, Munich, Thomas Sartorius, Jan Aachen, Schulte, and Hamburg, "Method and arrangement for spectral broadening of laser pulses for non-linear pulse compression," United States Patent US9847615 B2 (19 December 2017).
40. S. C. Pinault and M. J. Potasek, "FREQUENCY BROADENING BY SELF-PHASE MODULATION IN OPTICAL FIBERS," *J. Opt. Soc. Am. B* **2**(8), 1318–1319 (1985).
41. T. Nagy, P. Simon, and L. Veisz, "High-energy few-cycle pulses: post-compression techniques," *Advances in Physics: X* **6**(1), 1 (2021).
42. N. Daher, F. Guichard, S. W. Jolly, X. Délen, F. Quéré, M. Hanna, and P. Georges, "Multipass cells: 1D numerical model and investigation of spatio-spectral couplings at high nonlinearity," *J. Opt. Soc. Am. B* **37**(4), 993 (2020).
43. M. Kaumanns, D. Kormin, T. Nubbemeyer, V. Pervak, and S. Karsch, "Spectral broadening of 112 mJ, 1.3 ps pulses at 5 kHz in a LG10 multipass cell with compressibility to 37 fs," *Opt. Lett.* **46**(5), 929–932 (2021).
44. J. Song, Z. Wang, R. Lv, X. Wang, H. Teng, J. Zhu, and Z. Wei, "Generation of 172 fs pulse from a Nd: YVO₄ picosecond laser by using multi-pass-cell technique," *Appl. Phys. B* **127**(4), 50 (2021).
45. J. Song, Z. Wang, X. Wang, R. Lü, H. Teng, J. Zhu, and Z. Wei, "Generation of 601 fs pulse from an 8 kHz Nd:YVO₄ picosecond laser by multi-pass-cell spectral broadening," *Chin. Opt. Lett.* **19**(9), 093201 (2021).